Journal of Power Sources 185 (2008) 1049–1055

Contents lists available at ScienceDirect

Journal of Power Sources

journal homepage: www.elsevier.com/locate/jpowsour

# Stability study of cermet-supported solid oxide fuel cells with bi-layered electrolyte

Xinge Zhang[a,*], Javier Gazzarri[a], Mark Robertson[a], Cyrille Decès-Petit[a], Olivera Kesler[b]

[a] National Research Council, Institute for Fuel Cell Innovation, 4250 Wesbrook Mall, Vancouver, BC, Canada V6T 1W5
[b] Department of Mechanical and Industrial Engineering, University of Toronto, 5 King's College Road, Toronto, ON, Canada M5S 3G8

ARTICLE INFO

*Article history:*
Received 2 July 2008
Received in revised form 30 July 2008
Accepted 20 August 2008
Available online 2 September 2008

*Keywords:*
SOFC
Low temperature
Stability
Bi-layered electrolyte
SDC
SSZ

ABSTRACT

Performance and stability of five cermet-supported button-type solid oxide fuel cells featuring a bi-layered electrolyte (SSZ/SDC), an SSC cathode, and a Ni-SSZ anode, were analyzed using polarization curves, impedance spectroscopy, and post-mortem SEM observation. The cell performance degradation at 650 °C in $H_2$/air both with and without DC bias conditions was manifested primarily as an increase in polarization resistance, approximately at a rate of 2.3 mΩ cm$^2$ h$^{-1}$ at OCV, suggesting a decrease in electrochemical kinetics as the main phenomenon responsible for the performance decay. In addition, the initial series resistance was about ten times higher than the calculated resistance corresponding to the electrolyte, reflecting a possible inter-reaction between the electrolyte layers that occurred during the sintering stage. *In situ* and *ex situ* sintered cathodes showed no obvious difference in cell performance or decay rate. The stability of the cells with and without electrical load was also investigated and no significant influence of DC bias was recorded. Based on the experimental results presented, we preliminarily attribute the performance degradation to electrochemical and microstructural degradation of the cathode.



## 1. Introduction

The benefits of ceria as an electrolyte material in solid oxide fuel cells include higher ionic conductivity and better compatibility with the high performance mixed ionic and electronically conductive (MIEC) cathode materials than the conventional zirconia-based electrolytes. However, these benefits of ceria-based electrolytes are partially offset by its considerable electronic conductivity under certain operating temperature and atmospheric conditions. This phenomenon results in an electronic current flowing across the electrolyte, leading to a reduction in open circuit voltage, fuel utilization, and electrical efficiency [1]. One way to alleviate this problem is to coat the ceria-based electrolyte with a thin layer of stabilized zirconia, thus blocking the flow of electrons [2]. For example, Yahiro et al. [3] added a thin (1.5 μm) protective layer of yttria-stabilized zirconia (YSZ) on the fuel side of a yttria-doped ceria electrolyte (1.5 mm) supported solid oxide fuel cell (SOFC), increasing the open-circuit voltage (OCV) and enhancing power density. This type of cell is commonly called a bi-layered electrolyte SOFC. Using an anode supported cell structure with thin YSZ/samaria-doped ceria (SDC) bi-layered electrolyte deposited by electrophoretic deposition [4] and by conventional wet processing [5], a peak power density of 0.6 W cm$^{-2}$ at 700 °C has been reported. Recently, we demonstrated higher performance of cells with scandia-stabilized zirconia (SSZ)/SDC bi-layered electrolytes. We obtained a peak power density of 0.85 W cm$^{-2}$ and an OCV of 1.02 V at 700 °C using a combined tape casting, screen printing and co-firing technique [6], and a peak power density of 0.95 W cm$^{-2}$ and an OCV of 1.04 V at 600 °C using pulsed laser deposition [7]. Although the bi-layered electrolyte cell strategy has successfully prevented internal shorting in ceria-based electrolyte cells and has enabled compatibility with high-performance MIEC cathodes [8], cell performance stability has scarcely been reported in the literature. In the present contribution, we study performance and stability of cermet-supported button cells with bi-layered SSZ/SDC electrolytes.

## 2. Experimental procedure

### 2.1. Button cell preparation and testing

Table 1 shows the cell materials and the geometrical characteristics of our cells. Details of the cell preparation were given elsewhere [6]. Five cells of the same composition and the same anode and

* Corresponding author. Tel.: +1 604 221 3077.
*E-mail address:* xinge.zhang@nrc.ca (X. Zhang).

0378-7753/$ – see front matter. 
doi:10.1016/j.jpowsour.2008.08.070

**Table 1**
Cell materials, thicknesses, and processing conditions

| Cell component | Material | Thickness [μm] | Process | Firing condition |
|---|---|---|---|---|
| Cathode | $Sm_{0.5}Sr_{0.5}CoO_{3-y}$ (SSC) | 40–50 | Stencil printing | Cells A, B and C: *in situ* at 650 °C for 1.5 h; Cells D and E: *ex situ* at 1000 °C for 2 h |
| Electrolyte | $Sm_{0.2}Ce_{0.8}O_{1.9}$ (SDC) | 5 ± 1 | | |
| | $Sc_{0.2}Ce_{0.01}Zr_{0.79}O_{1.9}$ (SSZ) | 3 ± 1 | Screen printing | 1400 °C, 2 h |
| Anode | NiO–SSZ | 10–15 | | |
| Substrate | NiO–YSZ | 800–1000 | Tape casting | |

**Table 2**
Testing characteristics of the five bi-layered electrolyte button cells

| Cell # | Time elapsed until each EIS measurement [h] | Remarks | |
|---|---|---|---|
| A | 0, 0.33, 6, 6.84 | Excursion to 800 °C between 0.33 and 6 h. Held at 0.75 V while not measuring EIS. | Performance evaluation |
| B | 0, 0.33, 90, 115, 138, 144 | Excursion to 1000 °C between 138 and 144 h. | Constant voltage, then no current (see Table 4) |
| C | 1, 53, 150, 216, 218, 306 | Held at 0.5 A $cm^{-2}$ for 150 h, then OCV for 156 h. | Constant current |
| D | 0, 0.16, 2, 89 | Held at OCV throughout the test. | No current |
| E | 0, 100 | Held at 0.70 V throughout the test. | Constant voltage |

electrolyte fabrication process, and cathode deposition process, were labelled A, B, C, D and E in this report. After deposition of the cathode layer, cells A, B, and C were mounted on a test jig and were heated at 5 °C $min^{-1}$ to 650 °C and held for the reduction of the anode layer along with the *in situ* sintering of the cathode layer. The hydrogen partial pressure on the anode side was gradually increased (10, 20, 40, 60, and 100% $H_2$, balance $N_2$, at 15 min intervals) to reduce the NiO to Ni. The anode reduction and cathode *in situ* sintering time was approximately 1.5 h. The anode fuel stream, with a flow rate of 100 ml $min^{-1}$, passed first through a bubbler humidifier before entering the anode chamber, while ambient air (100 ml $min^{-1}$) flowed on the cathode side. In cells D and E, the cathode was pre-fired *ex situ* at 1000 °C for 2 h, and then coated with a wet layer of SSC to ensure good electrical contact against the current collecting mesh. In all cells, the cathode geometrical area was 0.5 $cm^2$. Impedance measurements were performed at 650 °C at OCV with a perturbation amplitude of 50 mV. The frequency ranged from 0.1 Hz to 100 kHz, with 10 data points per decade. Polarization and impedance were measured over time at 650 °C, with an intermediate excursion to 800 °C in cell A and to 1000 °C in cell B, and a pre-test excursion to 700 °C in cells D and E. Table 2 indicates the testing characteristics.

## 3. Results and discussion

### 3.1. Test results

Figs. 1–13 show the DC and impedance behaviour of the five cells, taken at different times after anode reduction. The cell performance showed deterioration at times longer than 7 h, primarily manifested as an increase in polarization resistance near OCV. Cell C also showed a 20% increase in series resistance.

#### 3.1.1. Cell A

This cell was not subjected to stability testing. It was tested with the purpose of measuring the cell performance at different temperatures and the performance evolution during the initial several hours after the anode reduction process at 650 °C. During the 0.33–6 h period, the cell was heated up to 800 °C and cooled down to 550 °C at 50 °C intervals, measuring the polarization curve at each temperature. The detailed cell performance results and microstructure analysis have been published previously [6]. Table 3 gives a brief summary of the cell performance as a function of temperature. The cell reached a peak power density of 1.8 W $cm^{-2}$ at 800 °C, and of 0.5 W $cm^{-2}$ at 650 °C with OCV ranging from 0.99 to 1.04 V over the 550–800 °C temperature range.

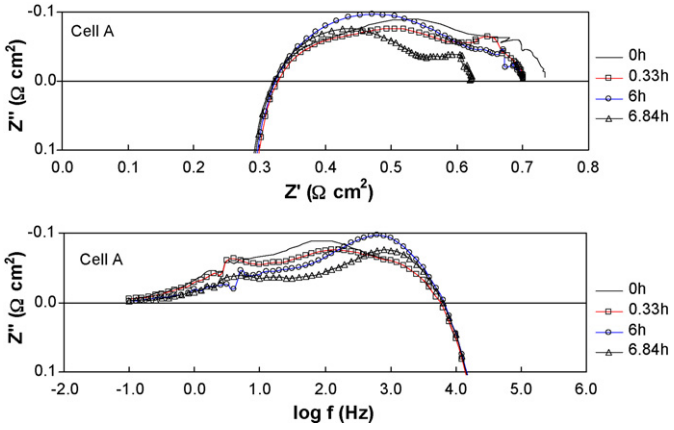


**Fig. 1.** Nyquist plot of the impedance evolution of cell A, tested at OCV at 650 °C. (Top) Nyquist plot. (Bottom) Imaginary impedance vs. frequency. The legend on the right indicates the time in hours elapsed since the beginning of the test. Between 0.33 and 6 h, the cell temperature was increased up to 800 °C and decreased back to 650 °C.

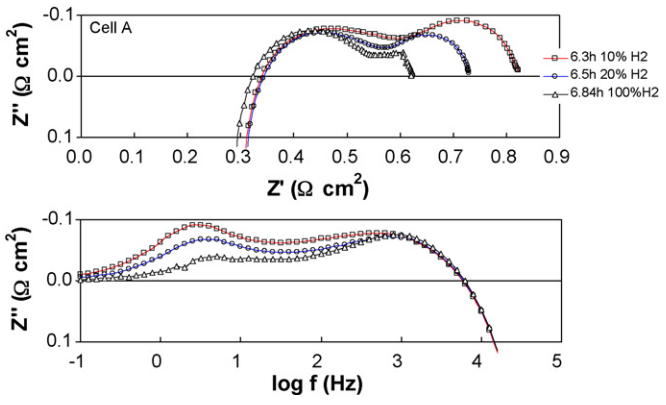


**Fig. 2.** Influence of $H_2$ dilution on the cell impedance. (Top) Nyquist plot. (Bottom) Imaginary impedance vs. frequency. The low frequency process shows a strong dependence on hydrogen activity, and thus we attribute it to the anode. Testing conditions: 650 °C, OCV, 10, 20 and 100% $H_2$, balance $N_2$/air (total gas flow rates for both anode and cathode are 100 ml $min^{-1}$).

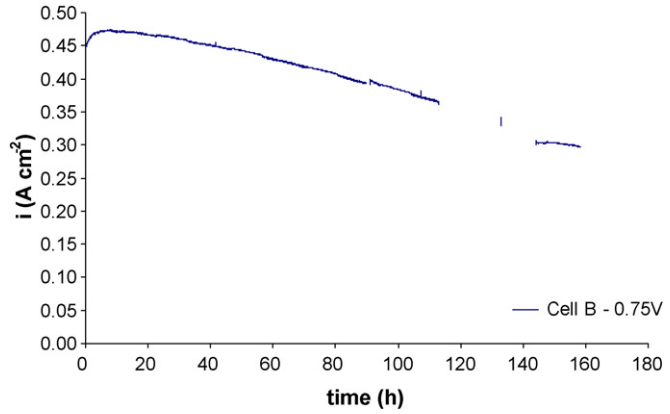


**Fig. 3.** Current density delivered by cell B as a function of time, in potentiostatic mode at 0.75 V. After a short activation period, the performance decays steadily throughout the testing time.

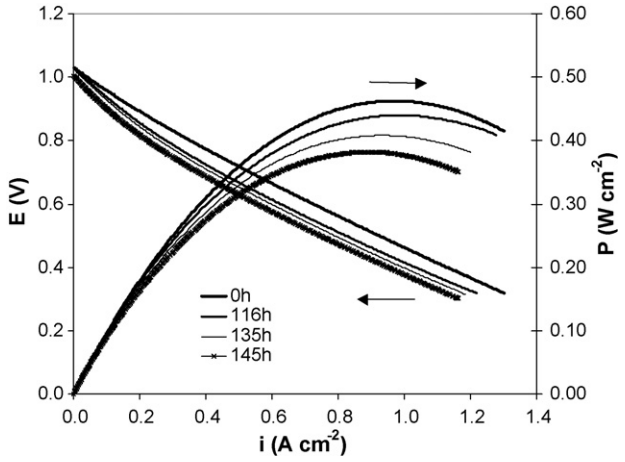


**Fig. 4.** *I–V* and power density curves showing the time evolution of the electrochemical performance of cell B. The decay is more significant below 0.3 A cm$^{-2}$ than it is at high polarizations. Legend indicates time elapsed in hours.

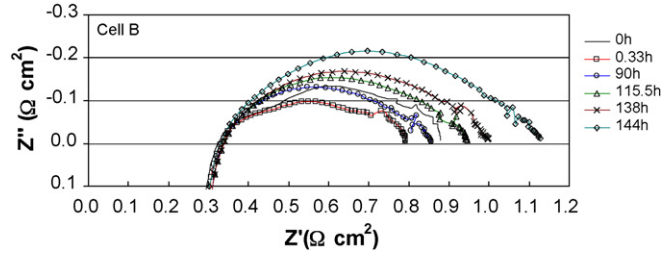


**Fig. 5.** Nyquist plot of the impedance evolution of cell B, taken at OCV at 650 °C. An excursion to 1000 °C took place between 138 and 144 h. Legend indicates time elapsed in hours.

**Table 3**
Initial performance of cell A as a function of temperature

| $T$ [°C] | OCV [V] | $P_{pk}$ [W cm$^{-2}$] |
|---|---|---|
| 550 | 1.04 | 0.13 |
| 600 | 1.04 | 0.28 |
| 650 | 1.03 | 0.50 |
| 700 | 1.02 | 0.85 |
| 750 | 1.01 | 1.33 |
| 800 | 0.99 | 1.80 |

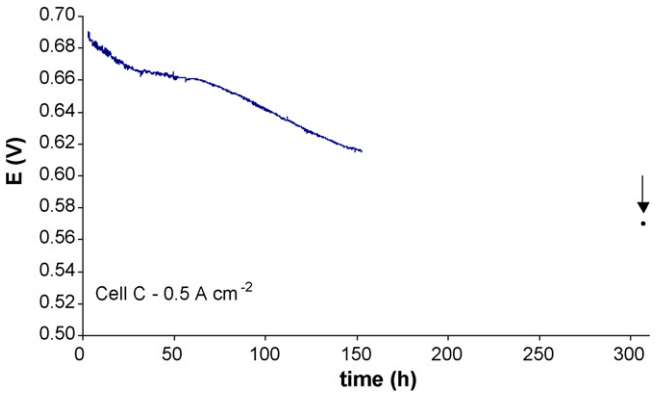


**Fig. 6.** Potential delivered by cell C as a function of time, in galvanostatic mode at 0.5 A cm$^{-2}$. The data point indicated with the arrow was calculated based on the polarization curve obtained at 307 h.

Fig. 1 shows the impedance results of this cell at 650 °C recorded at different times. The labels indicate the times at which the impedance measurement started. The evolution of the impedance spectrum in Fig. 1(top) shows some performance improvement with time. Generally, this behaviour is attributed to the completion of the anode reduction (a process with sluggish kinetics at 650 °C), and initial electrochemical improvement of the cathode [9].

Changing the hydrogen partial pressure of the anode feed gas helped understanding individual contributors to cell polarization. Fig. 2 shows the result of changing the hydrogen concentration at the anode of cell A. The labels in the figure indicate the conditions and times at which the impedance measurements were performed. It is apparent that the low frequency process (with relaxation peak frequency in the range from 1 to 10 Hz) is the most affected by

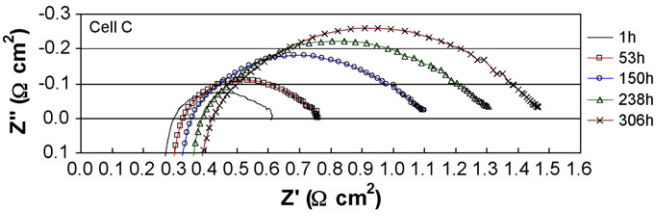


**Fig. 7.** Nyquist plot of the impedance evolution of cell C, at OCV at 650 °C. An excursion to 0.75 V (OCV = 0.983 V) took place after 53 h.

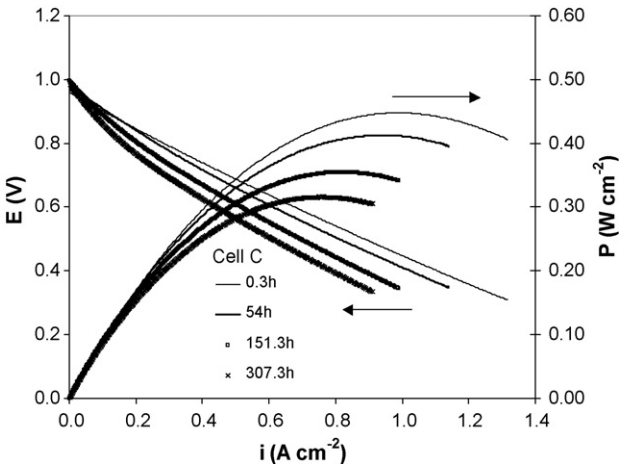


**Fig. 8.** *I–V* and power density curves showing the time evolution of the electrochemical performance of cell C. Legend indicates time elapsed in hours.

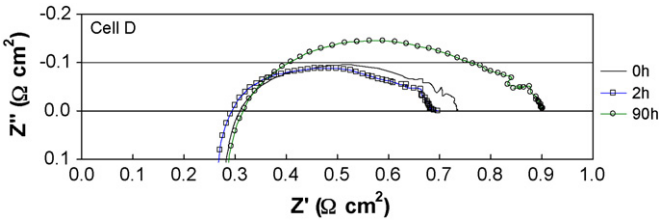


**Fig. 9.** Nyquist plot of the impedance evolution of cell D at OCV at 650 °C. The cell temperature was increased to 700 °C before the first test indicated as 0 h.

hydrogen concentration, while the high frequency process (with relaxation peak frequency in the 100–1000 Hz range) is not substantially affected. Thus, the low frequency arc is related to the anode process. Verbraeken et al. [10] reported a similar peak frequency range in their symmetric Ni–YSZ anode cell at 800 °C with $H_2$ fuel. They found two processes with relaxation peak frequencies of approximately 20 and 0.1 Hz contributing to the anode electrochemical process. In addition, we have compared the cathode relaxation frequencies in this data set with those of symmetric cells consisting of SSC cathodes on SDC electrolytes, and found both to appear within the 100–1000 Hz range. Therefore, we link the high frequency arc mainly to the cathode process.

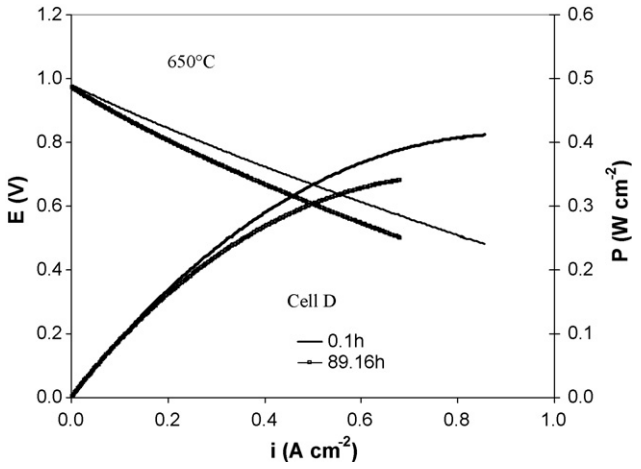


**Fig. 10.** *I–V* and power density curves showing the time evolution of the electrochemical performance of cell D. Legend indicates time elapsed in hours.

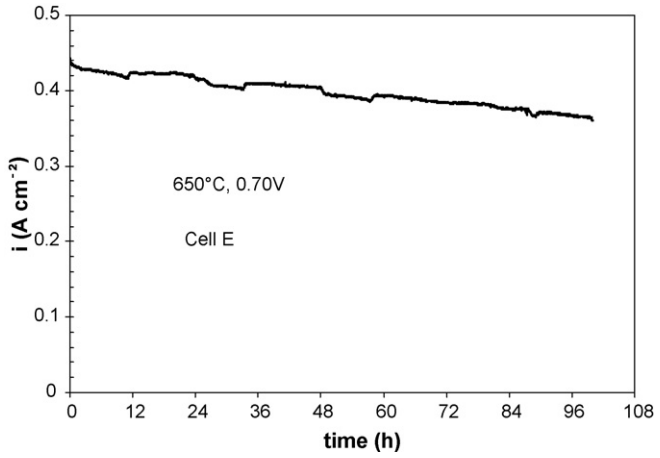


**Fig. 11.** Current density delivered by cell E as a function of time, in potentiostatic mode at 0.70 V.

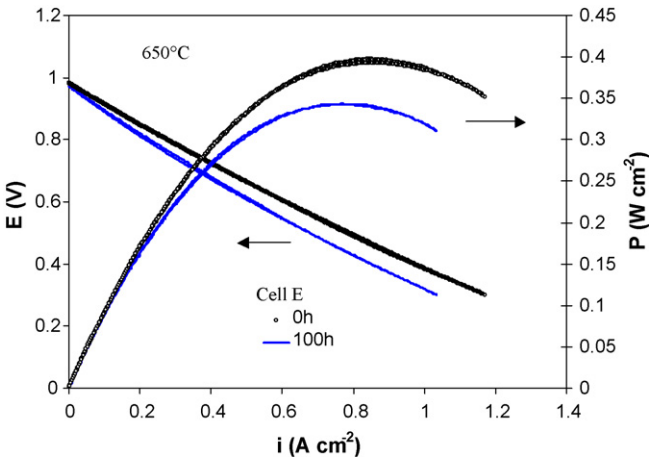


**Fig. 12.** *I–V* and power density curves showing the time evolution of the electrochemical performance of cell E. Legend indicates time elapsed in hours.

The imaginary impedance vs. frequency plot given in Fig. 1(bottom) reveals that the relaxation frequency changes with time mostly in the high frequency range. In electrodes with RC behaviour, the peak frequency depends inversely on the electrode polarization resistance, $R_p$. Decreasing the value of $R_p$ will cause an increase in the peak frequency if the capacitance of the electrochemical double layer is constant. The peak frequency of the cathode process does increase with time during this test, providing further evidence of an improvement in the cathode process. Therefore, the performance improvement of cell A over the first 7 h is mostly related to a decrease in the cathode polarization resistance. Similarly, with decreasing $H_2$ concentration, a small shift of relaxation peak frequency to lower frequency is observed as depicted in Fig. 2(bottom), indicating an increase in the anode polarization resistance with the decrease in the anode hydrogen concentration. Finally, Fig. 2(top) also reveals that there is an increase in series resistance, $R_s$, with the decrease in hydrogen concentration. It would be reasonable to expect the ceria layer of the electrolyte to become less conductive with decreasing $H_2$ concentration at the anode, since the conductivity of ceria is decreased under higher $p_{O_2}$ at the anode side. Although we add the dense SSZ layer at the anode side, a change in conductivity could still occur due to pinholes or micro-cracks in the SSZ layer that allow the anode reactant to be in contact with

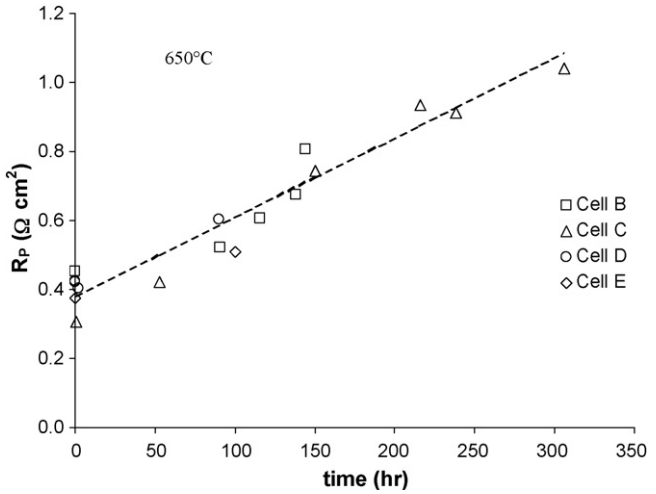


**Fig. 13.** Polarization resistance evolution with time for cells B, C, D and E. Average $R_p$ increase is 2.3 mΩ cm² h⁻¹.

**Table 4**
A summary of the performance and degradation rates of cell B

| Time [h] | 0 | 7 | 50 | 113 | 138 | 144 | 158.5 |
|---|---|---|---|---|---|---|---|
| $i$ [A cm$^{-2}$] | 0.450 | 0.473 | 0.443 | 0366 | 0.341 | 0.303 | 0.297 |
| Degradation rate [mA cm$^{-2}$ h$^{-1}$] | / | −3.28 | 0.70 | 1.20 | 1.25 | / | 0.44 |
| Comment | ← 0.75 V → | | | ← OCV, 850–550 °C → | | ← Heat to 1000 °C → | ← 0.75 V → |

SDC. In fact the OCV value (1.03 V) of the cells is slightly lower than the theoretical Nernst potential (1.15 V), suggesting the presence of such micro-defects in our cells.

### 3.1.2. Cell B

Figs. 3–5 show electrochemical testing results for cell B. This cell has been tested under potentiostatic operation at 0.75 V for approximately 113 h after the cell reduction at 650 °C. Consistently with what had been observed in cell A, Figs. 3 and 5 show a small improvement in cell performance during the first 7 h after cell reduction. While held for 113 h at a constant voltage of 0.75 V at 650 °C, this cell showed a decay of approximately 0.92 mA cm$^{-2}$ h$^{-1}$ after the initial cell performance improvement (Fig. 3). After 113 h of potentiostatic operation at 0.75 V, the cell was held at OCV for 20 h during the test period of 113–133 h. The calculated degradation rate at OCV was 1.25 mA cm$^{-2}$ h$^{-1}$, determined from the decrease in current density at 0.75 V between $I$ and $V$ curves measured over that test period. During the period of 133–138 h, the cell temperature was varied up to 850 °C and back down to 550 °C for performance–temperature measurement. Subsequently, the cell was heated up to 1000 °C and held for 2 h to improve cathode sintering over 138–144 h, then returned to 0.75 V potentiostatic operation at 650 °C for another 14 h with a calculated degradation rate of 0.44 mA cm$^{-2}$ h$^{-1}$. Table 4 summarizes the main results and degradation rates for the different periods.

The DC polarization curves (Fig. 4) revealed a larger performance deterioration below 0.3 A cm$^{-2}$ than above that current density. Since activation polarization governs the region close to OCV, the decay is likely related to an electrochemical kinetic loss of the electrode processes. The complex impedance evolution (Fig. 5) shows an initial convolution of at least three arcs that coalesced over approximately 90 h into a single depressed arc, followed by a constant shape size increase. The peak frequency decreased slightly over the 150–250 Hz range. That range is attributable to the cathode process, as stated in Section 3.1.1. Thus, the performance decay can be attributed to an increase in cathode polarization resistance. *In situ* sintering the cathode at a higher temperature (1000 °C) improved the performance stability in the later hours of the test (144–158 h); however, an OCV loss of 18 mV from 1.022 to 0.994 V and a performance loss of 0.038 A cm$^{-2}$ from 0.341 to 0.303 A cm$^{-2}$ at 0.75 V were observed after the heat treatment at 1000 °C for 2 h.

### 3.1.3. Cell C

Cell C was tested at a constant current density of 0.5 A cm$^{-2}$ for over 150 h, then left at OCV for another 157 h at 650 °C without any additional temperature excursion. The results are shown in Fig. 6, showing a voltage decay of 0.07 V (from 0.69 V down to 0.62 V) with a nonlinear time dependence under constant current density. The average decay rate at 0.5 A cm$^{-2}$ was 0.47 mV h$^{-1}$, and the average decay rate at OCV was approximately 0.32 mV h$^{-1}$, calculated based on the total cell voltage drop (from 0.62 to 0.57 V) at 0.5 A cm$^{-2}$. This cell was the only one to show an obvious increase in series resistance during impedance testing as shown in Fig. 7. However, its increase in polarization resistance was far larger. Like cell B, the complex impedance showed an early stage coalescence of multiple arcs (at least two in the case of cell C) into one depressed arc, followed by further shape-invariant growth. Increasing polarization resistance with time was also observed with $I$–$V$ curves having more rapid slope increase at low rather than high DC polarization conditions, as seen in Fig. 8. The trend in peak frequency was similar to that observed in cell B, indicating that the cathode performance loss was the main contributor to decay.

### 3.1.4. Cell D

Cell D was held at OCV for approximately 90 h after cell reduction, and showed a similar decay in performance as cells B and C, i.e. a shape-preserving impedance arc growth (Fig. 9). Based on our results of a reduced degradation rate for cell B after *in situ* 1000 °C sintering, we expect with *ex situ* sintered cathode (1000 °C for 2 h in air) the cell stability could be improved. However, neither the rate of decay nor the initial performance and initial ohmic loss were significantly different from those of the other cells. Fig. 10 shows the $I$–$V$ and power density curves of cell D at the starting point (0 h) and the ending point (90 h) of the test at 650 °C. The average decay rate was calculated based on the $I$–$V$ results shown in Fig. 10, resulting in 0.84 mV h$^{-1}$ under 0.5 A cm$^{-2}$ from 0.68 to 0.605 V, or 0.78 mA cm$^{-2}$ h$^{-1}$ under 0.75 V from 0.35 to 0.28 mA cm$^{-2}$.

### 3.1.5. Cell E

We tested another cell (cell E) with an *ex situ* sintered cathode to further clarify the influence of DC bias on cathode stability. This cell was tested under potentiostatic operation at 0.70 V for 100 h at 650 °C. Fig. 11 shows the current density change with time. This cell showed an OCV of 0.982 V (see Fig. 12), and the degradation rate was 0.73 mA cm$^{-2}$ h$^{-1}$ over a 100 h period, from 0.436 to 0.363 A cm$^{-2}$. Interestingly, the OCV values of cells D and E with *ex situ* sintered cathodes were slightly lower (0.98 V) than those of the other cells. As described before for cell B, a similar OCV loss was also observed after heating up to 1000 °C during the final period of testing (see Fig. 4 and Table 2). Two mechanisms may be responsible for this change: the sintering of the cathode layer may generate thermal stresses in the electrolyte, leading to increased micro-crack and pinhole density, and/or cobalt may diffuse into the electrolyte layer and promote mixed conductivity of the bi-layered electrolyte. Both processes would lead to a Nernst potential loss, and possibly also a partial reduction of the ceria in the SDC layer, with its consequent increase in electronic conductivity and internal shorting. Further investigation of the possible mechanism is needed. Cell E did not show a sign of stability improvement as we had anticipated.

## 4. Discussion

### 4.1. Incubation period

All cells in this test showed some initial performance improvement. We will refer to this initial stage as the incubation period. Typical signs are an initial decrease of the $R_p$ at OCV (Figs. 1, 5, and 9) during which the cell performance increases. In cell A, the electrode polarization resistance $R_p$ drops from 0.44 (0 h) to 0.32 Ω cm$^2$ during the first 6.84 h, while the series resistance $R_s$ shows almost no change. As described in the experimental section, the test procedure allowed 1.5 h for cell reduction, followed by the

electrochemical measurements. Although after the nominal reduction period the OCV was 1.03 V at 650 °C, the impedance results in Fig. 1 reveal that the reduction of the cermet anode may have not been completed. The shrinking of the low frequency arc (anode) with time supports this statement. Comparing the low frequency impedance of the anode processes at different times, the reduction process seems to continue during the first approximately 7 h, with the plot in Fig. 3 suggesting that at that time, reduction is either complete or at least occurs more slowly than cell degradation processes. It is worth mentioning that after the measurement at 0.33 h, cell A was heated up to 800 °C for a temperature dependent performance test. Therefore, the cell must have experienced an accelerated reduction process during the 0.33–6 h period. The low frequency arc preserves its shape between 6 and 6.84 h. As revealed in Fig. 1, most of the improvement in the cell performance came from the high frequency arc, which might be related to cathode microstructural stabilization.

The incubation times for cell A and for cell B were approximately 7 h long, after which cell impedance reached a minimum (Fig. 1) and performance reached a maximum (Fig. 3). Cell C exhibited a much shorter incubation time (less than 3 h), while the incubation times for cells D and E were less than 2 h. It seems that the extent of this incubation period depends on the processing and testing times and temperatures and on the resulting starting electrode microstructures. We conclude that the observed incubation behaviour is attributable to the processes of anode reduction and cathode sintering, with both processes nearing completion after the first few hours at operating temperature.

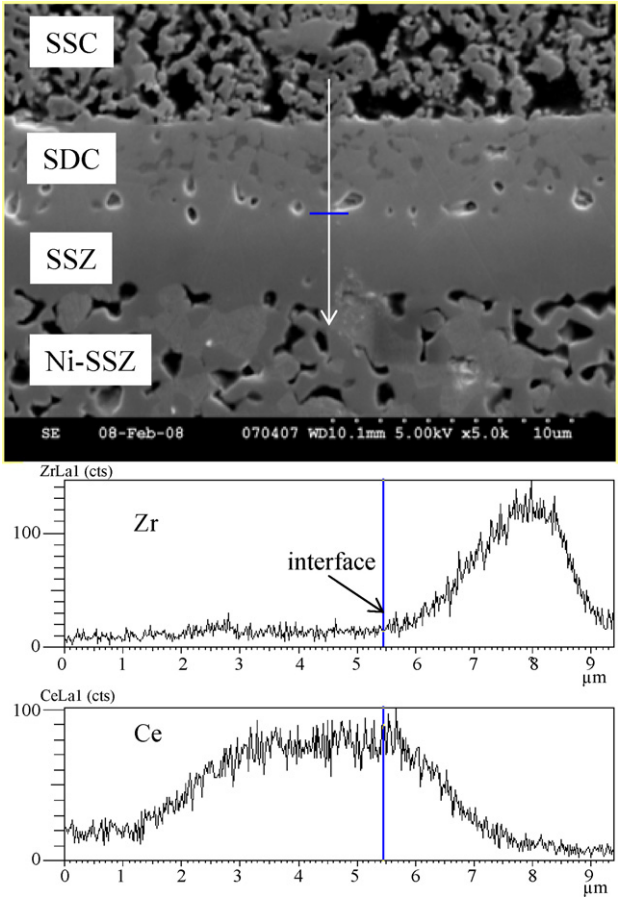


**Fig. 14.** (Top) SEM micrograph of the bi-layered electrolyte in contact with the electrodes of cell D. (Bottom) EDS results of Zr and Ce across the bi-layered electrolyte, the interface of two electrolytes is at 5.5 μm of the scan line.

**Table 5**
Summary of the cell resistances obtained in this work

| Cell | $R_s^0$ [Ω cm$^2$] | $R_s^{final}$ [Ω cm$^2$] | $R_p^0$ [Ω cm$^2$] | $R_p^{final}$ [Ω cm$^2$] |
|---|---|---|---|---|
| A | 0.32 | – | 0.42 | – |
| B | 0.33 | 0.34 | 0.42 | 0.61 |
| C | 0.30 | 0.36 | 0.31 | 0.74 |
| D | 0.31 | 0.31 | 0.43 | 0.59 |
| E | 0.33 | 0.34 | 0.38 | 0.51 |

Superscript 0 corresponds to initial conditions and final values correspond to 116 h for cell B, 150 h for cell C, 90 h for cell D, and 100 h for cell E at 650 °C and OCV.

### 4.2. Performance degradation

After performance stabilization, cells B, D, and E showed an increase in polarization resistance with no or very small change in series resistance. Cell C (Fig. 7) shows an increase in both series and polarization resistance, with the increase in series resistance, $R_s$, being much smaller than the increase in polarization resistance, $R_p$. Table 4 summarizes the $R_s$ and $R_p$ change during the first 90–150 h of testing time for the four stability test cells. It is clear that most of cells showed relatively stable $R_s$ values, of approximately 0.30–0.33 Ω cm$^2$ over the test periods. Only cell C showed a 20% increase in $R_s$ during the stability test. Fig. 13 shows the increase in polarization resistance for the four stability test cells. All four cells present comparable degradation trends. For example, the decay rate of cell C illustrated in Fig. 6 for the first 150 h at 0.5 A cm$^{-2}$ was 0.5 mV h$^{-1}$, while during 150–300 h at OCV, the decay rate was 0.3 mV h$^{-1}$, based on the change in voltage over these two test periods. Assuming that cathode microstructural instability was the main cause of degradation, we had expected that with (1000 °C, 2 h) *ex situ* sintered cathode, the performance stability might be improved. However, cells D and E, featuring *ex situ* sintered cathodes, degraded 0.78 mA cm$^{-2}$ h$^{-1}$ at OCV, and 0.73 mA cm$^{-2}$ h$^{-1}$ at 0.75 V, respectively. Figs. 3 and 6 also indicate that the performance decay of cells with *in situ* sintered cathodes is only mildly dependent on whether the cell was held under polarization or at OCV. Fig. 13 shows general consistency in the observed increase in $R_p$, largely independently of DC bias and cathode sintering strategy, and averaging 2.3 mΩ cm$^2$ h$^{-1}$ at OCV. Similar conclusions were reported by Becker et al. in their study of LSCF cathodes at 700 °C [11]. However, this observation contrasts with results reported in [12,13], where the authors point out that the decay rates depend on the current densities in YSZ electrolyte cells.

Comparing the recorded impedance spectra of all the cells, it is clear that the impedance increase within the 100–1000 Hz range is predominant over that at other frequencies. Based on the results and analysis above, we attribute most of the observed cell performance degradation to the cathode. A typical degradation mechanism affecting the cathode microstructure is chromium poisoning [14,15], a result of evaporation of chromium from stainless steel interconnectors. This phenomenon is ruled out in the present work, since no chromium-containing material is present at high temperature in our experimental setup. Two possible degradation mechanisms in this work are proposed: (1) coarsening of the microstructure due to sintering for the *in situ* sintered cathodes; (2) diffusion of strontium away from the SSC cathode, leading to strontium depletion that can significantly decreases the performance of cobaltite cathodes [16].

### 4.3. Bi-layered electrolyte resistance

From Table 5, the initial series resistance, $R_s^0$ taken as the initial high frequency intercept, is consistent throughout all the cells, with values ranging from 0.30 to 0.33 Ω cm$^2$, indicating good experimental repeatability. However, this value is well above the series

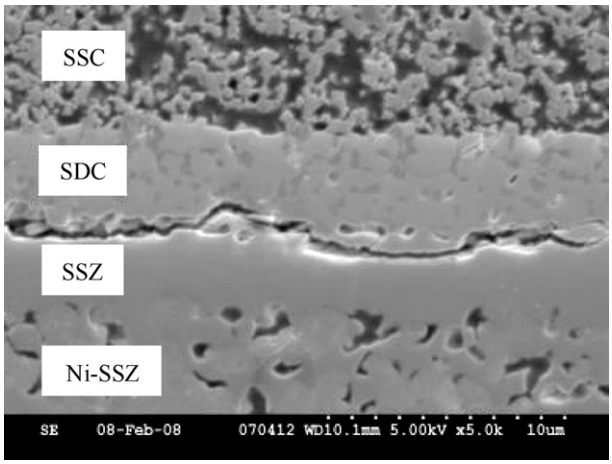


**Fig. 15.** Post-test SEM micrograph showing a delamination between the SSZ and SDC electrolyte layers in cell D. This separation was observed at several spots across the cell, and may have been partially responsible for the large initial series resistance observed in all specimens. It was not possible to determine the stage at which separation occurred; however, it is reasonable to state that this interfacial bond was weaker than those at the other interfaces were.

resistance calculated using the SDC thickness (4–6 μm) and SSZ thickness (2–4 μm) and conductivities (0.03–0.04 S cm$^{-1}$ for SDC [17] and 0.02–0.03 S cm$^{-1}$ for SSZ [18] at 650 °C). The theoretical $R_s$ for those cells based on the individual electrolyte layer thicknesses (5 μm SDC, 3 μm SSZ) is only approximately 0.03–0.04 Ω cm$^2$ in total. Therefore, the measured $R_s$ value of the bi-layered electrolyte is one order of magnitude higher than the theoretical resistance. As illustrated in SEM images (Fig. 14, top), while the SSZ layer showed high density after sintering, the SDC layer exhibited pores and voids that could partially contribute to the abnormally high initial series resistance observed in all cells due to a decrease in area of the conductive path through the electrolyte layers. Probably, the main cause of the high $R_s$ value is the formation of an inter-diffusion layer between the SDC and SSZ layers, most likely formed during the sintering stage [6,19], and resulting in a low conductivity zone in the bi-layered electrolyte. EDS results of Zr and Ce concentrations across the bi-layered electrolyte showed a clear diffusion of Ce into the SSZ layer (Fig. 14, bottom). It has been well reported that the Ce–Zr–O solid solution shows extremely low ionic conductivity [20], so that even an inter-diffusion layer of only 1–2 μm thick generate a large resistance in the oxide ionic conduction path. In addition, although most of the cell structure showed good adhesion between layers in post-mortem microstructural observation, we did observe some detached areas (Fig. 15). It is difficult to be certain about the stage at which this detachment occurred. However, it is logical to assume that this interface had been weakly bonded *a priori*. While all of these phenomena would have contributed to the higher observed values of $R_s$, they would also have had implications on the electrode electrochemical performance due to the shadowing effect that large voids or blocking layers have on cells with large aspect ratios [21,22]. The growing $R_s$ in the cell C test seems attributable to the possible detachment between the electrolyte layers during the cell testing.

In a future work we will analyze possible causes for the observed time-dependent decay in cell performance. We will analyze this phenomenon by considering several possible degradation modes via a numerical model of the cell performance in order to distinguish between different possible degradation modes. Possible candidates will include the loss in active surface area and/or of ionic conductivity of the cathode, and structural micro-delamination and void coalescence.

## 5. Conclusions

The stability tests (up to 300 h) of our cermet-supported button cells with bi-layered SSZ/SDC electrolytes resulted in continuous performance decay, mostly manifested as an increase in electrode polarization resistance. This observation, along with the frequency range at which most of the impedance growth is evident, led us to attribute the cell decay to a decrease in the cathode performance. Common observations were the initial change in the impedance arc shape from a multiple arc to a single depressed arc, followed by an increase in size with no further shape change.

The series resistance observed initially in all cells was invariably higher than the theoretical series resistance. The most likely cause for this observation is the presence of an inter-reaction layer between the electrolyte layers. Microscopic examination showed a weakened adhesion between the SDC and SSZ electrolyte layers, a phenomenon likely contributing to the high $R_s$. Sintering of the SSC cathode *ex situ* at 1000 °C did not result in any obvious performance difference, regardless of whether the cell was held at OCV or under polarization during the testing time.

## References

[1] X. Zhang, M. Robertson, C. Dces-Petit, W. Qu, O. Kesler, R. Maric, D. Ghosh, J. Power Sources 164 (2007) 668.
[2] K. Eguchi, T. Setoguchi, T. Inoue, H. Arai, Solid State Ionics 52 (1992) 165.
[3] H. Yahiro, Y. Baba, K. Eguchi, H. Arai, J. Electrochem. Soc. 135 (1988) 2077.
[4] M. Matsuda, T. Hosomi, K. Murata, T. Fukui, M. Miyake, J. Power Sources 165 (2007) 102.
[5] X. Zhang, M. Robertson, C. ces-Petit, Y. Xie, R. Hui, S. Yick, E. Styles, J. Roller, O. Kesler, R. Maric, D. Ghosh, J. Power Sources 161 (2006) 301.
[6] X. Zhang, M. Robertson, C. Decès-Petit, W. Qu, O. Kesler, R. Maric, d. Ghosh, J. Power Sources 175 (2008) 800.
[7] D. Yang, X. Zhang, C. Decès-Petit, R. Hui, R. Maric, d. Ghosh, J. Power Sources 164 (2006) 182.
[8] T.L. Nguyen, K. Kobayashi, T. Honda, Y. Iimura, K. Kato, A. Neghisi, K. Nozaki, F. Tappero, K. Sasaki, H. Shirahama, K. Ota, M. Dokiya, T. Kato, Solid State Ionics 174 (2004) 163.
[9] S. Koch, et al., Fuel Cells 6 (2) (2006) 117.
[10] M.C. Verbraeken, B.A. Boukamp, D.H.A. Blank, SOFC IX 2 (2005) 1218.
[11] M. Becker, A. Mai, E. Ivers-Tiffee, F. Tietz, SOFC IX 1 (2005) 514.
[12] M.J. Heneka, E. Ivers-Tiffee, SOFC IX 1 (2005) 534.
[13] A. Hagen, R. Barfod, P. Hendriksen, Y.-L. Liu, S. Ramousse, J. Electrochem. Soc. 153 (2006) A1165.
[14] S. Paulson, V. Birss, J. Electrochem. Soc. 151 (2004) A1961.
[15] E. Konysheva, et al., J. Electrochem. Soc. 153 (2006) A765.
[16] S.P. Simner, M.D. Anderson, M.H. Engelhard, J.W. Stevenson, Electrochem. Solid-State Lett. 9 (2006) A478.
[17] V.V. Kharton, F.M.B. Marques, A. Atkinson, Solid State Ionics 174 (2004) 135.
[18] J.W. Fergus, J. Power Sources 162 (2006) 30.
[19] N. Sakai, et al., Solid State Ionics 143 (2001) 151.
[20] A. Tsoga, A. Naoumidis, D. Stover, Solid State Ionics 135 (2000) 403.
[21] J.I. Gazzarri, O. Kesler, J. Power Sources 167 (2007) 430.
[22] J.I. Gazzarri, O. Kesler, J. Power Sources 176 (2008) 155.